

Coherent radio pulses from showers in different media: A unified parameterization

Jaime Alvarez-Muñiz, Enrique Marqués, Ricardo A. Vázquez, and Enrique Zas
*Departamento de Física de Partículas and Instituto Galego de Física de Altas Enerxías,
Universidade de Santiago de Compostela, E-15782 Santiago de Compostela, Spain*

We study the frequency and angular dependences of Cherenkov radio pulses originated by the excess of electrons in electromagnetic showers in different dense media. We develop a simple model to relate the main characteristics of the electric field spectrum to the properties of the shower such as longitudinal and lateral development. This model allows us to establish the scaling of the electric field spectrum with the properties of the medium such as density, radiation length, Molière radius, critical energy and refraction index. We normalize the predictions of the scaling relations to the numerical results obtained in our own developed GEANT4-based Monte Carlo simulation, and we give a unified parameterization of the frequency spectrum and angular distribution of the electric field in ice, salt, and the lunar regolith, in terms of the relevant properties of the media. Our parameterizations are valid for electromagnetic showers below the energy at which the Landau-Pomeranchuk-Migdal effect starts to be relevant in these media. They also provide an approximate estimate of radio emission in hadronic showers induced by high energy cosmic rays or neutrinos.

PACS numbers: 95.85.Bh, 95.85.Ry, 29.40.-n

I. INTRODUCTION

Neutrinos are the most suitable candidates to extend astronomical observations to the ultra high energy (UHE) regime, above ~ 1 TeV. Unlike charged particles, they point directly to the source where they were produced. Unlike neutrons, they are stable. Unlike photons, they can penetrate large amounts of matter, and they are not attenuated by cosmic backgrounds. They are not optimal candidates though, due to their small interaction cross section, and to their small expected fluxes at ultra high energy [1, 2, 3]. However these two latter difficulties may be overcome with a large enough detector volume of at least 1 km^3 [4].

The “conventional” technique to achieve a large detector volume exploits the observation of Cherenkov light emitted by high energy neutrino-induced muons and showers in water and ice [5, 6, 7, 8, 9]. An alternative to it is the search for coherent Cherenkov radio pulses in the MHz-GHz radio frequency range, produced by neutrino induced showers in dielectric, transparent, dense media. When the wavelength of the emitted radiation is larger than the typical dimensions of the shower the emission is coherent. The contribution to the electric field from positive and negative particles would approximately cancel out were it not for the existence of an excess of electrons over positrons in the shower [10]. The charge asymmetry arises from photon and electron scattering on the surrounding medium that sweeps electrons into the shower, and from positron annihilation in flight that contributes to the excess charge by terminating positron trajectories. Due to the coherent nature of the radio emission the power in radio waves scales as the square of shower energy.

Dense media have the advantage that shower dimensions are of the order of meters, and coherence extends to high frequencies, typically $\sim \text{GHz}$, where more power

is available because the coherently radiated electric field is proportional to frequency. Besides, large formations of dense, transparent media such as ice and salt exist in nature having attenuation lengths in radio frequencies of a few hundred meters [11, 12, 13]. They have the advantage of being located in low noise environments such as the South Pole or deep salt mines. A single antenna in such a medium makes a detector of effective volume of $\sim 0.1 \text{ km}^3$ water equivalent [14, 15]. The cost-effectiveness of antennas also adds to the attractiveness of the radio technique.

Several experiments are searching for neutrinos exploiting the radio technique in dense media. The RICE experiment [16] is an array of antennas buried in the Antarctic ice cap that has imposed stringent limits on astrophysical neutrino fluxes in the energy range above $\sim 10^{17}$ eV [17]. The Goldstone Lunar Experiment (GLUE) has used two large radiotelescopes to search for pulses produced by neutrino-induced showers on the Moon’s regolith [18]. With no neutrino candidates in 120 hours of observation, GLUE has established competitive upper bounds on astrophysical neutrinos of energy above $\sim 10^{19}$ eV [19]. The technique could be of interest to search for ultrahigh energy cosmic rays [20, 21] and is being explored using the Westerbork array of radiotelescopes in the Netherlands [22]. It will also be exploited by the proposed LUNASKA experiment in Australia [23]. A recently approved experiment is ANITA [24], a balloon-borne antenna that circles the Antarctic continent scanning for large radio pulses. The idea of using large salt domes as targets for neutrino interactions has also been explored and there is a proposed experiment named SalSA [25], as well as other initiatives such as the ZESANA proposal in the Netherlands [13].

It is also very important to remark that the dominant emission mechanism in dense media has been experimentally confirmed in accelerator measurements at SLAC,

using bunches of bremsstrahlung photons as projectiles, and sand and salt as target medium [26, 27]. This experiment has tested the theoretical predictions originally made by Askar'yan in the 1960's [10].

Given the current and future experimental efforts, the motivation and aim of our work are clear: A good understanding and comprehensive characterization of the dependence of the radio signal on frequency and observation angle in different dense media are needed to interpret the data that is being collected [17, 19], as well as to evaluate the capabilities and potential of the planned experiments looking for neutrinos and cosmic rays.

In this paper we show that many of the observables of the electric field spectrum emitted by an electromagnetic shower developing in dense media, scale to a few percent level with several properties of the media, such as density (ρ), radiation length (X_0), Molière radius (R_M), critical energy (E_c), and index of refraction (n). This scaling allows us to predict the properties of radio pulses in different media without performing time-consuming Monte Carlo simulations. Our work provides further insight into the close relation between shower development and radio emission, which may help designing future experiments exploiting the radio technique, as well as assessing the potential of those currently under construction.

This paper is structured as follows. In Section II we briefly review radio emission from electromagnetic showers. In Section III by means of a simple toy model we relate the main features of the radiopulse to general characteristics of shower development. This allows us to obtain the scaling of radiopulse with the relevant parameters of the medium. In Section IV we normalize these scaling relations using our own developed GEANT4-based Monte Carlo simulation [29, 30] to numerically calculate the electric field spectrum in ice, salt and the lunar regolith. We also give in this section unified parameterizations of our numerical results to be used in practical applications and establish their range of applicability.

II. THE RADIO PULSE SPECTRUM

We provide here a short review on Cherenkov radio emission from electromagnetic showers for the sake of completeness. Further information can be found in references [31, 32, 33, 34, 35].

The Fourier time-transform in the Fraunhofer limit of the electric field radiated by a charge q moving at constant velocity \vec{v} for an infinitesimal time interval $(t_1, t_1 + \delta t)$ starting at the position \vec{r}_1 is given by [32]:

$$\vec{E}(\omega, \vec{r}) = \frac{q\mu_r i\omega}{2\pi\epsilon_0 c^2} \frac{e^{ikr}}{r} e^{i\omega(t_1 - \frac{n}{c}\hat{k}\cdot\vec{r}_1)} \vec{v}_\perp \delta t \frac{\sin y}{y} \quad (1)$$

with $y = \pi\nu\delta t(1 - n\beta\cos\theta)$. Here ϵ_0 (c) is the permittivity (speed of light) in vacuum, μ_r (n) is the relative magnetic permeability (the refraction index) of the medium,

ω the angular frequency, \hat{k} is a unit vector in the direction of observation, and \vec{v}_\perp is the projection of \vec{v} in the direction perpendicular to \hat{k} . r is the distance from the charge to the observer's position. It is straightforward to deduce Eq. (1) from the inhomogeneous Maxwell's equations in the transverse gauge for a point charge current [32, 36], keeping only the R^{-1} radiation term.

Eq. (1) displays the most important characteristics of the radiation emitted by a charged particle travelling along a straight trajectory at a speed larger than the speed of light in the medium:

1. The electric field spectrum rises linearly with frequency, and has a $\sin y/y$ term, where $y \propto \nu\delta t(1 - n\beta\cos\theta)$ that corresponds to an angular diffraction pattern peaked at the Cherenkov angle θ_c given by $\cos\theta_c = (n\beta)^{-1}$. The first zeros of the diffraction pattern happen at,

$$\Delta\theta \simeq \frac{1}{\nu\delta t\sqrt{n^2\beta^2 - 1}}, \quad (2)$$

that is the width of the peak around the Cherenkov angle is proportional to the inverse of the length of the particle's track, and to the inverse of the frequency of observation, as corresponds to the diffraction pattern produced by a single slit. For observation at the Cherenkov angle there is no phase factor associated to the position of the particle along the track and the maximum in the diffraction pattern is achieved [46].

2. The electric field is proportional to the length of the particle track perpendicular to the direction of observation, i.e. it scales as $\nu\delta t \sin\theta$.
3. The field is 100% polarized in the plane containing the observation direction and the particle trajectory.

In order to calculate the electric field produced by a shower, the contributions from each particle track, as given by Eq. (1), have to be summed taking into account their relative phases which stem from their different spacetime positions and different $\vec{\beta}$. To do this numerically, the tracks can be subdivided in small steps so that \vec{v} is approximately constant in each step.

The contribution to the total electric field from the particle tracks in a shower is strongly dependent on observation angle and frequency. The problem resembles a classical problem of interference in which the source emits in a coherent fashion as long as the wavelength of observation is insensitive to (i.e. larger than) the fine details of the emitting region. Further information on the characteristics of the electric field can be found in references [33, 34, 35, 37, 38, 39]. In Fig. 1 we show the results of our own developed GEANT4-based simulation of the electric field spectrum emitted by a 10 TeV shower in ice [30]. The spectrum is plotted for different observation

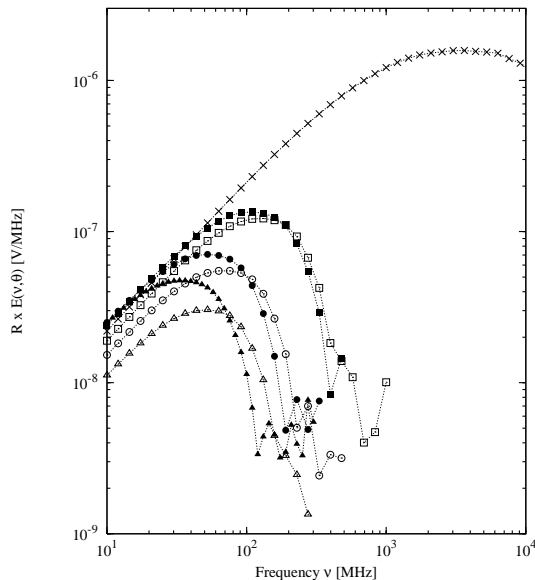


FIG. 1: Frequency spectrum of the electric field in ice observed at several angles from the shower axis: $\theta = \theta_c \simeq 55.8^\circ$ (crosses); $\theta_c + 10^\circ$ (bold squares); $\theta_c - 10^\circ$ (empty squares); $\theta_c + 20^\circ$ (bold circles); $\theta_c - 20^\circ$ (empty circles); $\theta_c + 30^\circ$ (bold triangles); $\theta_c - 30^\circ$ (empty triangles). The results were obtained using our own developed GEANT4-based Monte Carlo simulation. The lines joining the points are just to guide the eye.

angles θ with respect to shower axis. The electric field spectrum rises linearly with frequency up to a turnover point which depends on the observation angle.

III. TOY MODEL OF SHOWER DEVELOPMENT

In this section we describe a simple toy model of shower development that allows us to relate the main features of the electric field spectrum to the properties of the shower producing the field.

When a photon or electron of energy E incides on a thick absorber it initiates an electromagnetic shower. The number of electrons, positrons and photons in the shower rapidly grows due to bremsstrahlung and pair production which are the dominant processes at high energy. The energy of the primary particle initiating the shower quickly degrades because it is shared among an increasing number of secondaries, until their energy reach the so-called critical energy E_c , at which other processes become important, and electrons are as likely to lose all their energy through ionization as to radiate hard bremsstrahlung photons. As a result of the shower development, the number of particles increases up to a maximum N_{\max} , and exponentially decreases after it. Using the Heitler model [40] that assumes that in each interaction the energy is shared equally between the two secondaries, it is straightforward to show that

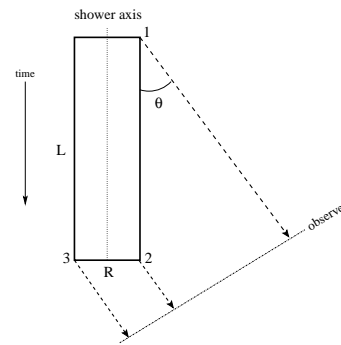


FIG. 2: Toy model of a shower. L is the effective length of the shower proportional to the radiation length L_0 and R is the shower width, proportional to the Molière radius R_M .

$N_{\max} = 2^p = E/E_c$, where p is the number of interactions before the shower reaches its maximum. Furthermore, in this model electrons and photons are assumed to travel a radiation length $L_0 = X_0/\rho$ before interacting. As a consequence the total tracklength T due to the charged particles in a photon initiated shower can be approximated by [28],

$$T \sim (2 + 2^2 + \dots + 2^p)L_0 \simeq N_{\max} L_0 = \frac{E}{E_c} \frac{X_0}{\rho}. \quad (3)$$

The particles in the shower also spread in the transverse dimension – perpendicular to shower axis – mainly due to multiple scattering. We can view a shower as a thin pancake of particles travelling at the speed of light ($\beta = 1$) along a length $L = k_L L_0 = k_L X_0/\rho$ proportional to the radiation length (Fig. 2). The pancake has a lateral width $R = k_R R_M/\rho$ proportional to the Molière radius R_M , the typical scale of the lateral spread of the shower (Fig. 2). Both k_L and k_R are normalization constants of the model to be determined in numerical simulations (see below).

This very simple model of shower development, as shown below, allows us to establish the relation between the frequency, angular distribution and absolute magnitude of the electric field, and the parameters of the medium in which it is emitted.

A. Electric field spectrum: shape

The overall time duration of the radio pulse for a given observation angle from shower axis (θ) is an exceedingly important parameter. It is related to the turnover frequency at which the spectrum departs from a linear behavior with frequency. There are two relevant time scales in our simple toy model, namely, δt_L the time delay between two light rays emitted at the two end points in the longitudinal development of the shower (points 1 and 2 in Fig. 2), and δt_R the time delay between two rays emitted from the two ends of the lateral spread of the shower (points 2 and 3 in Fig. 2). The dominance of one or the

other delay – i.e. the time duration of the pulse – depends on the observation angle. It is straightforward to obtain that:

$$\delta t_L = \frac{L}{c} (1 - n \cos \theta) = \frac{n}{c} \frac{k_L X_0}{\rho} (\cos \theta_c - \cos \theta), \quad (4)$$

where we have used $\cos \theta_c = 1/n$, and

$$\delta t_R = \frac{R}{c/n} \sin \theta = \frac{n}{c} \frac{k_R R_M}{\rho} \sin \theta. \quad (5)$$

For observation at the Cherenkov angle all the rays emitted along L at the same radial distance to the shower axis arrive at the same time at the observer, i.e. δt_L vanishes at $\theta = \theta_c$. Only the time delay associated to the lateral spread of the shower remains and the electric field spectrum increases linearly with frequency up to a turnover frequency given by

$$\nu_R(\theta = \theta_c) \simeq \frac{1}{\delta t_R} = \frac{\rho}{k_R R_M} \frac{c}{\sqrt{n^2 - 1}}. \quad (6)$$

where we have used $\sin \theta_c = \sqrt{1 - \cos^2 \theta_c} = \sqrt{n^2 - 1}/n$.

The corresponding turnover frequency associated to δt_L is,

$$\nu_L(\theta) \simeq \frac{1}{\delta t_L} = \frac{\rho}{k_L X_0} \frac{c}{|1 - n \cos \theta|}. \quad (7)$$

For observation away from the Cherenkov angle both $\delta t_R(\theta)$ and $\delta t_L(\theta)$ do not vanish. Eq. (4) illustrates the fact that $\delta t_L(\theta)$, the effective time duration of the longitudinal spread of the shower as viewed by the observer, grows from zero as the observation angle departs from θ_c , and equals δt_R for observation angles $\theta_+ = \theta_c + \delta\theta_+$ and $\theta_- = \theta_c - \delta\theta_-$ given by the condition $\delta t_L(\theta_\pm) = \delta t_R(\theta_\pm)$. For small values of $\delta\theta_\pm$,

$$\delta\theta_\pm \simeq \frac{k_R R_M \sin \theta_c}{k_L X_0 \sin \theta_c \mp k_R R_M \cos \theta_c}. \quad (8)$$

As a result, if $\theta \in (\theta_-, \theta_+)$, the shower electric field loses its full coherence at a turnover frequency ν_R determined mainly by the *lateral* spread of the shower and given by an equation similar to Eq. (6) but for an arbitrary θ . Correspondingly, if θ falls outside the (θ_-, θ_+) interval, the turnover frequency in the spectrum ν_L is determined by the *longitudinal* shower development, and is given by Eq. (7). As a limiting case of Eq. (8), in a shower having $L \gg R$, $\delta\theta_\pm \sim R/L \ll 1$ and the interference from different stages in the *longitudinal* shower development dominates the spectrum at essentially all angles, as expected in a one dimensional shower where L is the only relevant scale.

The width of the angular distribution of the electric field around the Cherenkov angle is given by an equation similar to Eq. (2) with an effective δt which is also proportional to L . As a result it is easy to infer that it scales as

$$\Delta\theta = \frac{c}{\nu} \frac{\rho}{k_\Delta X_0} \frac{1}{\sqrt{n^2 - 1}}. \quad (9)$$

Here k_Δ is a normalization constant to be determined in Monte Carlo simulations. Its numerical value is expected to be different from k_L , despite the fact that both the turnover frequency of the spectrum away from the Cherenkov angle, and the angular distribution of the pulse are mainly determined by the longitudinal development of the shower.

B. Electric field spectrum: magnitude

The absolute normalization of the field at low frequencies – in the fully coherent region where the electric field increases linearly with frequency – is known to be determined by the distance travelled by the excess charge along the perpendicular to the direction of observation. Using the expression for the tracklength in Eq. (3), the absolute normalization of the electric field for an observation angle θ is expected to scale as

$$r|\vec{E}| \sim k_E \nu T \sin \theta \simeq k_E \frac{E}{E_c} \frac{X_0}{\rho} \nu \sin \theta, \quad (10)$$

where k_E is a normalization constant to be determined in numerical simulations (see below), and r is the distance from the source to the observer. It is important to notice that we are implicitly assuming that particles travel parallel to shower axis. As a consequence, the projection of the tracks in the perpendicular to the direction of observation is simply accounted for by a factor $\sin \theta$ in Eq. (10).

IV. RADIO PULSE SPECTRUM IN DIFFERENT MEDIA

A. Radio pulse simulations in dense media

Using our own developed GEANT4-based Monte Carlo code [29, 30], we have simulated electromagnetic showers in ice, salt and the lunar regolith. These media are suitable targets in which neutrino interactions can be efficiently detected. It is worth remarking that we have checked these simulations against the ZHS Monte Carlo [32], an independent code whose results were shown in [30] to agree with those of GEANT4 to a few percent level in ice. Table I lists the relevant properties of the three media adopted in this work.

In Fig. 3 we show the frequency spectrum of the electric field emitted by a 10 TeV electromagnetic shower observed at the Cherenkov angle and at $\theta = 90$ deg. in ice, salt and the Moon's regolith, as obtained in our GEANT4-based simulations. In Fig. 4 we plot the angular distribution of the electric field at 100 MHz and 1 GHz. It is obvious by inspection that the shape of the frequency spectrum is fairly universal, only the normalization and the turnover frequency in the spectrum change from medium to medium and scale with its properties, as will be quantitatively shown in the next subsection.

TABLE I: Some relevant properties of the materials considered in this work: density ρ , radiation length X_0 , Molière radius R_M , critical energy E_c , and index of refraction at radio frequencies n . Last column is the energy above which the Landau-Pomeranchuk-Migdal effect starts to affect shower development using the definition in [42].

Medium	ρ [g cm ⁻³]	X_0 [g cm ⁻²]	R_M [g cm ⁻²]	E_c [MeV]	n	E_{LPM} [TeV]
Ice	0.92	36.08	10.35	73.0	1.78	~ 2400
Salt	2.05	22.16	12.09	38.5	2.45	~ 660
Moon	1.80	22.59	11.70	40.0	1.73	~ 770

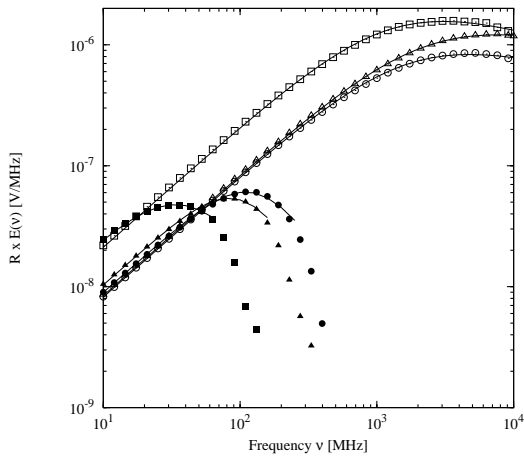


FIG. 3: The frequency spectrum of the electric field emitted by a 10 TeV shower in the direction of the Cherenkov angle and at 90 degrees in different dense media. Empty squares: ice, $\theta = \theta_c$; empty circles: salt, $\theta = \theta_c$; empty triangles: lunar regolith, $\theta = \theta_c$. Filled squares: ice, $\theta = 90$ deg.; filled circles: salt, $\theta = 90$ deg.; filled triangles: lunar regolith, $\theta = 90$ deg. The lines are the fits of the Monte Carlo results to Eqs. (11) and (12), using the values of the parameters in Table II.

B. A unified parameterization

From Eqs. (6), (7), (9) and (10), we have obtained a unified parameterization of the electric field spectrum and its angular distribution around the Cherenkov angle in terms of the relevant properties of the media that control radio emission. The electric field spectrum at the Cherenkov angle can be parameterized by the expression:

$$r|\vec{E}(\nu)|_{\theta_c} = k_E \frac{E}{E_c} \frac{X_0}{\rho} \frac{\nu}{1 \text{ MHz}} \sin \theta_c \frac{1}{1 + (\nu/\nu_R)^\alpha}, \quad (11)$$

where ν_R is given in Eq. (6). The parameterization is a good approximation to the electric field spectrum for frequencies typically below $\nu = 10$ GHz where coherent effects are still very important.

Away from the Cherenkov angle (i.e. for θ outside

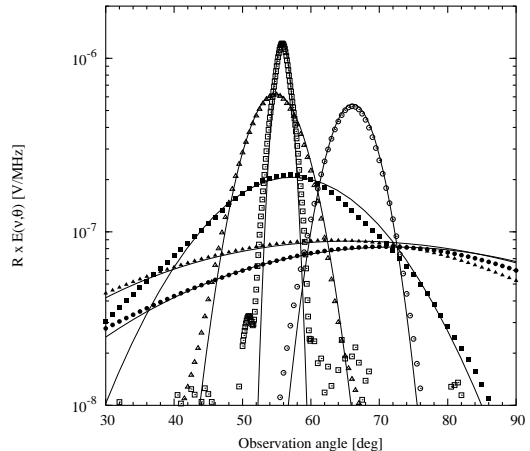


FIG. 4: Angular distribution of the electric field emitted by a 10 TeV shower in ice, salt and the lunar regolith. The distributions are shown at $\nu = 100$ MHz and $\nu = 1$ GHz. Empty squares: ice, $\nu = 1$ GHz; filled squares: ice, $\nu = 100$ MHz. Empty circles: salt, $\nu = 1$ GHz; filled circles: salt, $\nu = 100$ MHz. Empty triangles: lunar regolith, $\nu = 1$ GHz; filled triangles: lunar regolith, $\nu = 100$ MHz. The lines are the fits of the Monte Carlo results to Eq. (13) using the values of the parameters in Table II.

the interval (θ_-, θ_+) the electric field spectrum is well described by:

$$r|\vec{E}(\nu)|_{\theta} = k_E \frac{E}{E_c} \frac{X_0}{\rho} \frac{\nu}{1 \text{ MHz}} \sin \theta \frac{1}{1 + (\nu/\nu_L)^\beta}, \quad (12)$$

where ν_L is given in Eq. (7). This expression is generally valid up to frequencies $\sim 2\nu_L$. For larger frequencies, the fine structure of the shower is relevant (even at the individual particle level), and clearly our simplified toy model does not account for it.

The angular distribution of the pulse around the Cherenkov angle can be parameterized by a Gaussian peak modulated by a $\sin \theta$ which accounts for the angular behavior in the fully coherent region:

$$r|\vec{E}(\theta)| = r|\vec{E}(\nu)|_{\theta_c} \frac{\sin \theta}{\sin \theta_c} \exp \left[- \left(\frac{\theta - \theta_c}{\Delta \theta} \right)^2 \right], \quad (13)$$

with $\Delta \theta$ in radians given in Eq. (9).

In Eqs. (11), (12) and (13), k_E , k_L , k_Δ , k_R , α and β are parameters to be determined by fitting the results of Monte Carlo simulations of radiopulse emission in different media to the parameterizations. For this purpose, we have performed fits to the frequency spectrum at the Cherenkov angle and away from it, as well as to the angular distribution of the field around the Cherenkov angle, in ice, salt and the regolith using Eqs. (11), (12) and (13), and the numerical values of ρ , X_0 , R_M , E_c and n in Table I. Table II lists the results of these fits for the different media considered in this work. The fits are shown in Figs. 3 and 4.

As shown in Table II, it is remarkable that the numerical values of the normalization constants are weakly

TABLE II: Numerical values of k_E (in $\text{V cm}^{-1} \text{MHz}^{-2}$), k_L , k_Δ , k_R , α and β after fitting the results of Monte Carlo simulations to Eqs. (11), (12) and (13) in different media.

Medium	k_E	k_L	k_Δ	k_R	α	β
Ice	$4.79 \cdot 10^{-16}$	23.80	18.33	1.42	1.32	2.25
Salt	$3.20 \cdot 10^{-16}$	21.12	14.95	1.33	1.27	2.60
Moon	$3.30 \cdot 10^{-16}$	23.74	17.78	1.41	1.23	2.70

dependent on the medium. This is reflecting that most of the dependence on the medium is already accounted for in the unified parameterizations through the parameters ρ , X_0 , R_M , E_c and n . This is true at $\sim 40\%$ level in k_E , and at $\sim 15\%$ or less in the other normalization constants, which is remarkably good given the simplicity of our toy model of shower development in which the parameterizations are based.

The largest departure from being medium independent appears in k_E . The reason for this is that we made the simplification that particles in the shower follow straight lines parallel to the shower axis, while it is well known that they deviate from the shower axis by an average angle which is medium dependent. This dependence is not included in Eq. (10). As a result, the projection of the tracks in the perpendicular to the direction of observation is not simply accounted for by a factor $\sin\theta$, but some dependence on the deviation angle should be included in Eq. (10). The small departures from being medium independent in the other normalization constants can be attributed to the fact that an electromagnetic shower is better represented by a ‘‘cone’’ with medium-dependent opening angle, rather than by a ‘‘cylinder’’ as depicted in Fig. 2. This introduces an extra dependence on the medium which is not accounted for in Eqs.(6) and (7).

Finally, we are assuming in Eq. (3) that the electric field scales with the tracklength produced by particles with energy above the critical energy. However the electric field is known to scale with the excess charge tracklength, which is mainly due to Compton scattering dominating at energies below the critical energy. Using the total tracklength is however not a bad approximation because it scales in roughly the same way with medium parameters as the excess tracklength. This is confirmed by our GEANT4 simulations which predict a ratio of total to excess tracklengths with almost no dependence on the medium, of the order of 3.07, 3.05 and 2.98 in ice, salt and the lunar regolith, respectively.

C. Discussion: Range of applicability of the parameterizations

Eq. (11) together with the numerical values of the normalization constants k_E , k_R and α , describes accurately the electric field spectrum at the Cherenkov angle for frequencies below 10 GHz. This is well above the fre-

quencies of interest to experiments using ice, salt and the lunar regolith as targets for neutrino detection. The parameterization is also approximately valid at all energies, because the lateral dimension of the shower – responsible for the turnover frequency at the Cherenkov angle – does not change much with shower energy as Monte Carlo simulations of high energy showers in ice have confirmed [33, 37].

Away from the Cherenkov angle Eq. (12), together with the numerical values of the normalization constants k_E , k_L and β , describe accurately the electric field spectrum up to about twice the frequency at which the turnover in the spectrum occurs. However, contrary to Eq. (11), Eq. (12) is expected to fail at energies above the energy (E_{LPM}) at which the Landau-Pomeranchuk-Migdal effect [41] starts to affect the longitudinal shower development of the shower. The LPM effect is known to stretch the longitudinal development of an electromagnetic shower, and to change its effective longitudinal dimension. The LPM effect also produces a decrease of the turnover frequency in the spectrum as can be easily understood from Eq. (7) and was shown in [33]. In the last column of Table I we list E_{LPM} in ice, salt and the lunar regolith, using the definition of E_{LPM} in [42].

The angular distribution of the electric field around the Cherenkov angle in Eqs. (9) and (13), is also determined by the longitudinal development of the shower, and as a consequence it is also affected by the LPM effect. The parameterization in Eqs. (9) and (13) is only valid below E_{LPM} . It describes – with an accuracy of $\sim 10\%$ – the angular distribution of the electric field for frequencies above ~ 100 MHz, and in the angular range where the pulse falls by a factor ~ 2 -3 with respect to its value at the peak.

Our parameterizations are also expected to be a good approximation to the coherent Cherenkov radio emission in hadronic showers even at energies above E_{LPM} . Hadronic showers are known to be less affected by the LPM effect [37], and their efficiency of emission of coherent Cherenkov radiation at high energy has been shown to be similar to that of electromagnetic showers [43]. Besides, at high energy, a large fraction of the energy of the hadronic shower goes into its electromagnetic component [37]. Our parameterizations are then expected to be applicable in estimates of radio emission in most experiments looking for extremely high energy neutrinos. These experiments are currently concentrating most of their efforts on the detection of the hadronic showers produced in ν_μ charged current interactions, or in the neutral current interaction of any neutrino flavor. The observation of the electromagnetic shower produced in a ν_e charged current interaction is expected to be very difficult because the LPM effect shrinks the angular distribution of the electric field reducing dramatically the available solid angle for detection [44].

The important issues in the last two paragraphs above, call for simulations of electromagnetic and hadronic showers with energies above E_{LPM} in different dense me-

dia. We defer this work to a future paper [45].

Acknowledgments: We thank P. Gorham, S. Razzaque, D. Saltzberg, S. Seunarine, D. Seckel and D. Williams for many discussions on the topic of the paper. This work was supported by “Xunta de Galicia”

(PGIDIT05 PXIC 20604PN), by “Ministerio de Educación y Ciencia” (FPA 2004-01198) and by FEDER funds. J.A.-M. is supported by the “Ramón y Cajal” program. We thank CESGA, “Centro de Supercomputación de Galicia” for computer resources.

-
- [1] T.K. Gaisser, F. Halzen, and T. Stanev, *Phys. Rep.* **258**, 173 (1995); *Phys. Rep.* **271**, 355 (1995) (erratum).
- [2] J.G. Learned and K. Mannheim, *Ann. Rev. Nucl. Sci.* **50**, 679-749 (2000).
- [3] F. Halzen and D. Hooper, *Rep. Prog. Phys.* **65**, 1025 (2002).
- [4] F. Halzen, *Proc. Snowmass 94 on Nuclear and Particle Astrophysics and Cosmology*, eds. R. Kolb and R. Peccei (1994).
- [5] E. Andres *et al.*, *Nature* **410**, 441 (2001).
- [6] E. Andres, *et al.* [The AMANDA collaboration], *Astropart. Phys.*, **13**, 1 (2000).
- [7] F. Feinstein, *et al.* [ANTARES Collaboration], *Nucl. Phys. Proc. Suppl.* **70**, 445 (1999).
- [8] G. Domogatsky [BAIKAL Collaboration], *Nucl. Phys. Proc. Suppl.* **110**, 504 (2002).
- [9] C. Spiering, *J. Phys. G* **29**, 843 (2003).
- [10] G.A. Askar'yan, *Soviet Physics JETP* **14,2**, 441 (1962); *Soviet Physics JETP* **48**, 988 (1965).
- [11] P. Hobbs, *Ice Physics*, Clarendon Press, Oxford, (1974).
- [12] P.W. Gorham, *et al.* *Nucl. Instrum. Meth A* **490**, 476 (2002).
- [13] A.M. van den Berg *et al.* in Proceedings of the International ARENA Workshop 2005, *International Journal of Modern Physics A* in press.
- [14] P.B. Price, *Astropart. Phys.* **5**, 43 (1996).
- [15] G. M. Frichter, J. P. Ralston and D. W. McKay, *Phys. Rev. D* **53** (1996) 1684.
- [16] I. Kravchenko *et al.* [RICE Collaboration], *Astropart. Phys.* **19**, 15-36 (2003).
- [17] I. Kravchenko *et al.* [RICE Collaboration], *Astropart. Phys.* **20**, 195-213 (2003).
- [18] P. W. Gorham, K. M. Liewer, C. J. Naudet, D. P. Saltzberg and D. Williams, *AIP Conf. Proc.* **579** (2001) 177.
- [19] P. W. Gorham, C.L. Hebert, K. M. Liewer, C. J. Naudet, D. P. Saltzberg and D. Williams, *Phys. Rev. Lett.* **93**, 041101 (2003).
- [20] M.A. Markov and I.M. Zheleznykh, *Nucl. Instr. and Methods in Phys. Research* **A248**, 242 (1986).
- [21] J. Alvarez-Muñiz and E. Zas, in Proceedings of the RAD-HEP Conference, *AIP Conf. Proc.* **579** (2001), Eds. D. Saltzberg and P.W. Gorham.
- [22] J. Bacelar *et al.* in Proceedings of the International ARENA Workshop 2005, *International Journal of Modern Physics A* in press.
- [23] R. Protheroe *et al.*, <http://www.physics.adelaide.edu.au/astrophysics/LUNASKA/LUNASKA-www.html>
- [24] P. Miocionvic *et al.* in Proceedings of the International ARENA Workshop 2005, *International Journal of Modern Physics A* in press.
- [25] See for instance P. W. Gorham talk given at Aspen Center for Physics 2002 Winter Conference, <http://astro.uchicago.edu/~olinto/aspen/program>
- [26] D. Saltzberg *et al.*, *Phys. Rev. Lett.* **86**, 2802 (2001).
- [27] P.W. Gorham *et al.* *Phys. Rev. D* **72**, 023002 (2005).
- [28] H.R. Allan, *Progress in Elementary Particles and Cosmic Ray Physics* **10**, 171 (1971) (North Holland Publ. Co.).
- [29] <http://wwwinfo.cern.ch/asd/geant4/geant4.html>
- [30] J. Alvarez-Muñiz, E. Marqués, R.A. Vázquez and E. Zas, *Phys. Rev. D* **67**, 101303 (2003).
- [31] F. Halzen, E. Zas, T. Stanev, *Phys. Lett. B* **257**, 432 (1991).
- [32] E. Zas, F. Halzen, T. Stanev, *Phys. Rev. D* **45**, 362 (1992).
- [33] J. Alvarez-Muñiz, E. Zas, *Phys. Lett. B* **411**, 218 (1997).
- [34] R. V. Buniy and J. P. Ralston, *Phys. Rev. D* **65**, 016003 (2002).
- [35] S. Razzaque, S. Seunarine, D. Z. Besson, D. W. McKay, J. P. Ralston and D. Seckel, *Phys. Rev. D* **65**, 103002, (2002).
- [36] J.D. Jackson, *Classical Electrodynamics*. 2nd edition, John Wiley and Sons, Inc, 1975.
- [37] J. Alvarez-Muñiz, E. Zas, *Phys. Lett. B* **434**, 396 (1998)
- [38] J. Alvarez-Muñiz, R.A. Vázquez and E. Zas, *Phys. Rev. D* **61**, 023001 (1999).
- [39] J. Alvarez-Muñiz, R. A. Vázquez and E. Zas, *Phys. Rev. D* **62**, 063001 (2000).
- [40] W. Heitler, *The Quantum Theory of Radiation.*, reprinted by Dover Publications, N.Y. (1984) (3rd edition), from the original published by Oxford University Press (1954).
- [41] L. Landau and I. Pomeranchuk, *Dokl. Akad. Nauk SSSR* **92** (1953) 535; **92** (1935) 735; A.B. Migdal, *Phys. Rev.* **103** (1956) 1811; *Zh. Eksp. Teor. Fiz.* **32** (1957) 633 [*Sov. Phys. JETP* **5** (1957) 527].
- [42] T. Stanev, *et al.* *Phys. Rev. D* **25**, 1291 (1982).
- [43] S. Hussain and D.W. McKay, *Phys. Rev. D* **70**, 103003 (2004).
- [44] See Proceedings of the International ARENA workshop 2005, *International Journal of Modern Physics A*, in press.
- [45] J. Alvarez-Muñiz *et al.* in preparation.
- [46] Note that there exists an angle $\theta_c = \arccos(1/n\beta)$ if and only if $v > c/n$ i.e. the particle travels at a speed larger than the speed of light in the medium.